

High-brilliance ultra-narrow-band x-rays via electron radiation in colliding laser pulses

Q. Z. Lv,^{1,*} E. Raicher,^{2,†} C. H. Keitel,¹ and K. Z. Hatsagortsyan¹

¹Max-Planck-Institut für Kernphysik, Saupfercheckweg 1, 69117 Heidelberg, Germany

²Soreq Nuclear Research Center, 81800 Yavne, Israel

(Dated: May 19, 2022)

A setup of a unique x-ray source is put forward employing a relativistic electron beam interacting with two counter-propagating laser pulses in the nonlinear few-photon regime. In contrast to Compton scattering (CS) sources, the envisaged x-ray source exhibits an extremely narrow relative bandwidth of 10^{-5} to 10^{-4} , comparable to the x-ray free-electron laser (XFEL). The brilliance of the x-rays can be 2–3 orders of magnitude higher than a state-of-the-art CS source, while the angle spreading of the radiation is much smaller. By tuning the laser intensities and the electron energy, one can realize either a single peak or a comb-like x-ray source around keV energy. The laser intensity and the electron energy in the suggested setup are rather moderate, rendering this scheme compact and table-top size, as opposed to XFEL and synchrotron infrastructures.

Ever since the discovery by W. C. Röntgen in 1895, x-rays have introduced powerful techniques for determining the structure of matter at the atomic length scale. Continuous endeavours expanded the capabilities of x-rays over a wide range of disciplines spanning from physics to chemistry, biology, and material science [1, 2]. Remarkable advancements have been achieved with the employment of synchrotron radiation [3–6], which dramatically increased the brightness of the source, as well as with the introduction of the 4th generation light sources, in the form of the x-ray free-electron laser (XFEL) [7–12]. Unfortunately, the large size and cost of these facilities, limit their accessibility to a wide community.

Alternative schemes rely on Thomson- and Compton-scattering [13–16], and recently also on the radiation from laser-plasma interactions [17–20]. The advancement of compact and powerful laser systems revived interest to these sources [21–35]. The Compton scattering (CS) source is based on a collision of a laser pulse with a relativistic electron beam, as shown in Fig. 1(a). Though the peak brightness is lower than what can be obtained from large facilities mentioned above, CS sources have several advantages. They are relatively compact, affordable and easy to operate. Furthermore, they provide x-ray photons at a tunable energy in a broad spectral range.

A compact light source in the x-ray regime with improved brilliance and narrow bandwidth (BW) is attractive for many scientific communities, e.g., for x-ray imaging of objects in biology [36], x-ray scattering diagnostics for nanoscale samples [37–39] in material science, x-ray spectroscopy of highly charged ions [40, 41]. Recently a new field of x-ray quantum optics has been advanced aimed at the coherent control of atomic nuclei using shaped resonant x-rays [42–46], which requires especially narrow BW x-ray beams. Different schemes for narrowing the x-ray BW have been proposed involving temporal laser pulse chirping [28–32], or temporally varying polarization [33] to compensate the non-linear spectrum broadening due to the high field of the laser. Alternatively, with a low laser intensity (and low BW), the x-ray photon yield can be enhanced using a traveling-wave setup which allows an overlap of electron and laser beams longer than the Rayleigh length [34, 35]. However, all these approaches require the precise control of the pulse shape, phase or polarization, which is difficult especially

in the high intensity domain.

In this Letter an alternative approach for narrow BW bright x-rays is put forward. Rather than modifying the laser pulse, an additional laser beam co-propagating with the electrons is introduced. Namely, the setup consists of a relativistic electron beam interacting with two counterpropagating waves (CPW), see Fig. 1(b). The electron motion features two typical frequencies, separated by orders of magnitude because of the Doppler effect, $\omega_1 = \omega_0(1 + v_z)$, $\omega_2 = \omega_0(1 - v_z)$ where ω_0 is the laser frequency and v_z the relativistic average velocity on axis (units $\hbar = c = 1$ are used throughout). Due to the nonlinearity of the relativistic dynamics the electron absorbs several light quanta in both frequencies in the considered regime when emitting an x-ray photon. As a result in the emission spectrum the Doppler-shifted high frequency ω_1 peak is accompanied with satellites of ω_0 separation. While the gross features of the spectrum (the spectral envelope) are determined by the counterpropagating laser beam, the subtle features (BW of satellites) arise via the second co-propagating laser beam. Accordingly, the BW of satellites scales with the smaller frequency ω_2 . Consequently, this scheme allows for an ultra-narrow BW bright emission in the x-ray regime.

The emitted spectrum has been calculated employing the semiclassical operators method developed by Baier and Katkov [47], suitable for calculating QED processes of ultrarelativistic particles in strong background fields, when the electron dynamics is quasiclassical. The radiation spectrum reads [48, 49]:

$$dI = \frac{\alpha}{(2\pi)^2 T} \left[-\frac{\varepsilon'^2 + \varepsilon^2}{2\varepsilon'^2} |\mathcal{T}_\mu|^2 + \frac{m^2 \omega'^2}{2\varepsilon'^2 \varepsilon^2} |\mathcal{I}|^2 \right] d^3 \mathbf{k}', \quad (1)$$

where $\mathcal{I} \equiv \int_{-\infty}^{\infty} e^{i\psi} dt$ and $\mathcal{T}_\mu \equiv \int_{-\infty}^{\infty} v_\mu(t) e^{i\psi} dt$ with $\psi \equiv \frac{\varepsilon}{\varepsilon'} \mathbf{k}' \cdot \mathbf{x}(t)$ being the emission phase and $x_\mu(t)$, $v_\mu(t)$, $k'_\mu = (\omega', \mathbf{k}')$ the four-vectors of the electron coordinate, the velocity and the emitted photon momentum, respectively. τ is the pulse duration, ε the electron energy in the field, and $\varepsilon' = \varepsilon - \omega'$. In our setup ultrarelativistic electrons with an energy of $\varepsilon = 40m$ counter-propagate with the circularly polarized laser field $A_1(x, t) = m\xi_1[\cos(k_1 \cdot x)e_x + \sin(k_1 \cdot x)e_y]$, where $\xi_1 = eE_0/(m\omega_0)$ is the normalized field strength, E_0 and ω_0 are the laser field amplitude and frequency, respectively, $k_1 = (\omega_0, 0, 0, -\omega_0)$

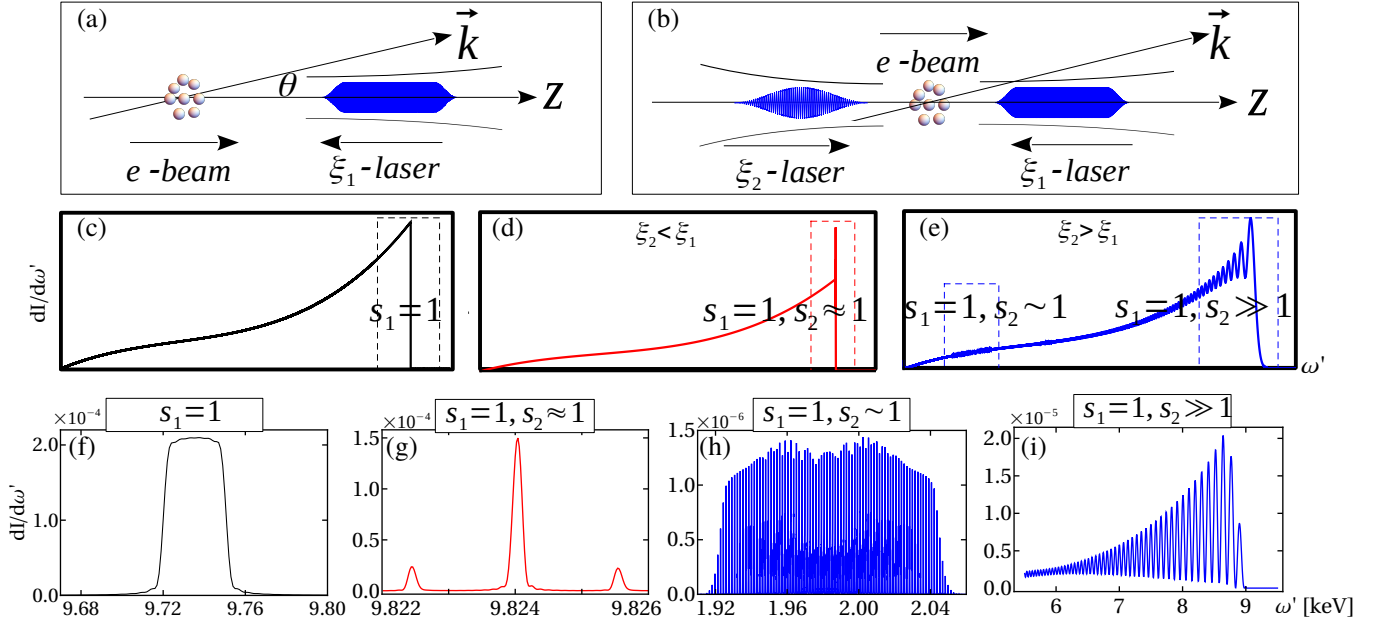


Figure 1. Upper panel: the setup of Compton scattering for a relativistic electron beam colliding with a single laser pulse (a) and colliding with a CPW (b); Middle panel: the sketch of the emission spectra for CS (c) and for an electron in CPW with $\xi_1 > \xi_2$ (d) and $\xi_1 < \xi_2$ (e); Lower panel: the zoom-in spectra for different cases. Panel (f) for CS with the emitted angle θ in an interval of 0.1 mrad around ξ_1/γ , and (g) for an electron in CPW with $\xi_1 > \xi_2$ having on-axis emission with $\theta \leq 0.1$ mrad and (h) with $\xi_1 < \xi_2$ having on-axis emission with $\theta \leq 1$ mrad. For comparison, the spectrum for an electron in CPW with $\xi_1 < \xi_2$ but the emitted angle θ is around ξ_2/γ with 1 mrad spreading is shown in panel (i). The field strength is $\xi_1 = 0.1$ in all cases while $\xi_2 = 0.02$ for (g) and $\xi_2 = 2$ for (h) and (i). The electron energy is $\varepsilon = 40 m$ for all cases [(f)-(i)].

is the laser four-wave vector with $\omega_0 = 1.55$ eV, and $e_x = (0, 1, 0, 0)$, $e_y = (0, 0, 1, 0)$ are the unit vectors, and $-e$ and m are the electron charge and mass, respectively. The second laser field co-propagating with the electrons is also circularly polarized: $A_2(x, t) = m\xi_2[\cos(k_2 \cdot x)e_x + \sin(k_2 \cdot x)e_y]$, with the wave vector $k_2 = (\omega_0, 0, 0, \omega_0)$. The two lasers have the same frequency ω_0 in the lab frame. Regarding the field strength, we keep $\xi_1 < 1$, namely $\xi = 0.1$ in the considered example in Fig. 1, while choose either $\xi_2 < \xi_1$ ($\xi_2 = 0.02$) or $\xi_2 > \xi_1$ ($\xi_2 = 2$). The corresponding spectra are presented in Fig. 1(d,g) [case I (indicated with red color)] and (e,h,i) [case II (blue)], respectively. The quantum strong-field parameter $e\sqrt{-(F^{\mu\nu}P_\nu)^2}/m^3$, with the field tensor $F^{\mu\nu}$, and four-momentum P_ν , is very small $\chi \sim 10^{-5}$ for the chosen parameters. As a result, the radiation reaction due to multiple photon emissions is negligible.

Let us begin the discussion of the features of radiation spectra from the case of common CS, $\xi_2 = 0$, see Fig. 1(c) and (f). Since $\xi_1 < 1$, the spectrum has a very sharp edge corresponding to absorption of a single photon from the laser field. In order to obtain a relatively narrow BW, one can restrict the angle range of the radiation. Such a spectrum is presented in panel (f). The angle window was centred around $\theta = \xi_1/\gamma$, with the electron Lorentz factor γ , where the main emission is located [50].

In the considered CWP setup with the two lasers, the normalized acceleration χ is dominated by the first laser field in all cases, which determines the general shape of all spectra. However, the zoom-in of the spectra for the CPW case in Fig. 1(g),

(h) and (i) reveal features stemming from the second pulse as well, which are absent in CS, panel (f). In panel (g) a single but ultra-narrow harmonic rises with a similar location and strength as for the CS in panel (f). For case II, the entire spectrum becomes oscillatory, panel (e). In most of the energy domain these oscillations are quite wide, as seen also in panel (i). The radiation emitted on axis, however, which corresponds to $s_2 \sim 1$, exhibits a comb of sharp peaks, shown in panel (h).

The spectra in (g) and (h) are not only very narrow in energy domain but are also highly collimated, resulting in high brilliance. With the same electron beam parameters (1nC charge and 0.01% spreading at $\varepsilon \lesssim 100$ MeV) for the CPW case in panel (d) the peak brilliance is $\mathcal{B} \sim 2.72 \times 10^{23}$ ph/(s·mrad²·mm²·0.1%BW), which is three orders of magnitude larger than the CS in panel (f). The peak brilliance in panel (h) is also one order of magnitude larger than a CS even with the location far away from the main peak. Therefore, the CPW setup is capable of producing brighter and narrower radiation than a CS. Furthermore, the comb-like structure produced in the regime $\xi_2 > \xi_1$ [Fig. 1(h)] is very promising. While the state-of-art technique of frequency comb can achieve the XUV domain [51–54], the covet is the hard x-ray regime. An attempt in this direction recently shown in [33] via CS with a polarization gating, demonstrated a relative BW of 10^{-2} and the spacing between peaks of hundreds of keV. In the setup presented here, on the other hand, we can achieve the comb spacing at an optical frequency, with a three orders of magnitude smaller relative

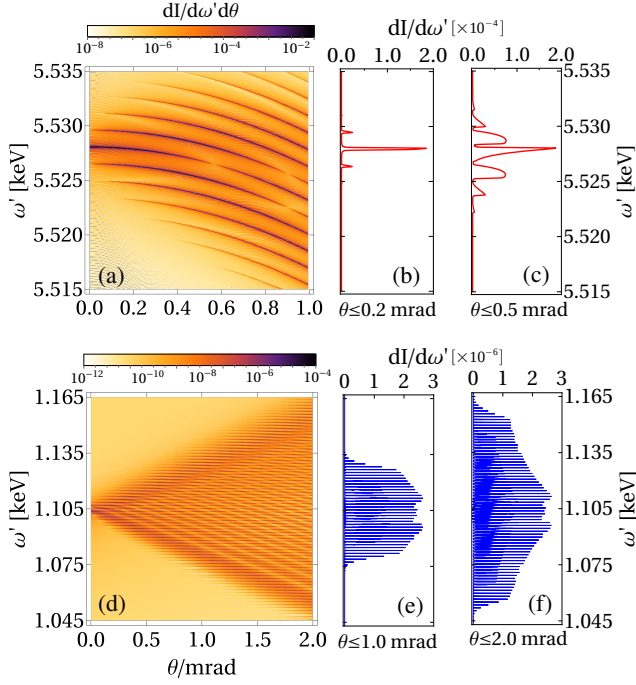


Figure 2. The angle resolved spectrum: (a) case I with $\xi_1 = 0.1$ and $\xi_2 = 0.02$; (b) and (c) are the spectra for the same parameters but integrated over different angle spreading, (b) for $\theta \leq 0.2$ mrad and (c) for $\theta \leq 0.5$ mrad. (d) case II with $\xi_1 = 0.1$ and $\xi_2 = 2$; the angle integrated spectra for this setup are shown in (e) for $\theta \leq 1.0$ mrad and (f) for $\theta \leq 2.0$ mrad. The radiation is symmetric with respect to the azimuthal angle and the spectra are integrated over it. The electron energy is $\varepsilon = 30m$ for both cases. The pulse length for ξ_1 is given by $N_1 = 80000$.

BW. Moreover, our method has the potential to shrink the comb spacing using a THz or microwave driving field for the ξ_2 wave.

The results in Fig. 1 raise several questions: i) What determines the peak locations and the spacing between sequential peaks? ii) What determines the width of a single peak? iii) What is the role played by the angle window? and iv) How can we control the number of harmonics contained in the spectrum? To address them, we turn to analytical estimations. Firstly, the BK phase can be written as $\psi = \psi_{np}t - z_1 \sin \omega_1 t - z_2 \sin \omega_2 t - z_3 \sin \Delta\omega_{12}t$ where $\psi_{np} = \varepsilon u(1 - v_z \cos \theta)$, $z_1 = (m\xi_1 u/\omega_1) \sin \theta$, $z_2 = (m\xi_2 u/\omega_2) \sin \theta$, $z_3 = 2\omega_0 m^2 \xi_1 \xi_2 u/(\varepsilon \Delta\omega_{12}^2)$, and $\Delta\omega_{12} = \omega_2 - \omega_1$. The integral in Eq. (1) over this phase yields multiplications of Bessel functions with arguments z_1, z_2, z_3 [55]. From the phase follows the energy-momentum conservation, determining the emitted photon energy [48, 49]:

$$\omega' = \frac{\omega_{s_1, s_2}^m}{1 + 2\gamma_*^2(1 - \cos \theta)}, \quad (2)$$

where $\omega_{s_1, s_2}^m = 2\gamma_*^2(s_1\omega_1 + s_2\omega_2)$ with s_1, s_2 being the numbers of photons absorbed from the first and second pulses, respectively, and $\gamma_* = \varepsilon/m_*$ with the effective mass $m_* \equiv m\sqrt{1 + \xi_1^2 + \xi_2^2}$ in the presence of CPW. The recoil term is suf-

ficiently small in the considered regime and thus is neglected. The spacing between sequential s_2 harmonics, according to Eq. (2), is $\Delta\omega' = 2\gamma_*^2\omega_2 \approx \omega_0$, as $\omega_1/\omega_2 \approx 4\gamma_*^2$ and $\omega_1 = 2\omega_0$.

To have a full picture of the emission, we depict in Fig. 2 the angle resolved spectra for both case I and II with $\varepsilon = 30m$. Panel (a) shows the spectrum for case I. Each line represents the location of a single harmonic with respect to ω_2 , in accordance with Eq. (2). The spacing between adjacent lines is ω_0 , as predicted above. One observes that the larger the angle range the more harmonics are included. Fig. 2(b) and (c) show the integration over two different ranges in θ domain of Fig. 2(a). For the CPW case the emission is nearly on axis ($\theta \sim 0$) [55], and can thus be confined to a small range $0 < \theta < \theta_w$. The resulting spectrum features a sharp cutoff for each harmonic, rendering their BW extremely narrow. The width of the harmonic due to this finite angle window based on Eq. (2) is [55]

$$\delta\omega'_w = \omega_{s_1, s_2}^m (\gamma_* \theta_w)^2. \quad (3)$$

For the common CS ($s_2 = 0$ in Eq. (2)), however, the main radiation is around ξ_1/γ [50]. In this region, the dependence on θ is stronger and thus $\delta\omega'_w$ is much larger, explaining the wide spectrum in Fig. 1(f), see also in [55].

Fig. 2(d) for case II is similar to Fig. 2(a). An analogous behaviour is observed with one obvious difference - the number of harmonics is significantly larger. We assess the effective number of harmonics Δs_2 for a given angle window θ_w by requiring $z_2/\Delta s_2 = \delta$, according to the governing Bessel function properties [55], with a choice of the small number $\delta \approx 0.8$:

$$\Delta s_2 \approx \frac{1}{\delta} \left(\frac{\theta_w}{\theta_c} \right), \quad \theta_c = \frac{m_*}{8m\xi_2 \gamma_*^3} \quad (4)$$

where θ_c corresponds to the angle when $\delta\omega'_w(\theta_c)$ is equal to the characteristic width of the harmonics discussed below. According to Eq. (4), the number of harmonics for case I is significantly lower as $m_*/m\xi_2 \approx \xi_1/\xi_2 \gg 1$. It should be mentioned that whereas the electron energy for both cases is essentially the same, the velocity along z -axis is larger in case I than that in case II (because of the different effective mass), rendering the photon energy ω' more sensitive to the emitted angle based on Eq. (2). The integrated spectra over a different angle range in panel (e) and (f) for case II reveals an interesting trade-off. On the one hand, the range of the comb can be extended by increasing the angle window, as also shown analytically above. On the other hand, it also induces a larger background in the gap between two sequential harmonics, which could destroy the comb-like structure. Namely, one should balance between the width of a single harmonic and the range of the total comb in an experiment to have an optimized x-ray comb in the keV regime.

In addition to the finite angle window discussed above, the width of the harmonics is affected by two other dynamical factors. The first stems from the characteristics of the electron dynamics. Relying on the features of the Bessel function in the spectrum, the width of the harmonics under consideration can be estimated from the requirement $z_2 \approx 1$, see [55]. For the

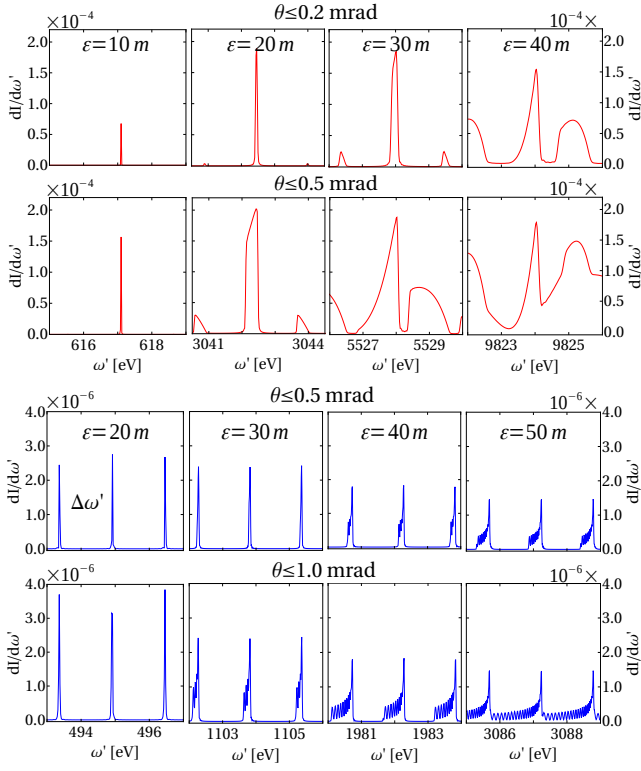


Figure 3. The spectral line's BW for different electron energies and different angle ranges: (upper panel, red curves) case I with $\xi_1 = 0.1$ and $\xi_2 = 0.02$; (lower panel, blue curves) case II with $\xi_1 = 0.1$ and $\xi_2 = 2$. The pulse length for ξ_1 is $N_1 = 80000$.

main peak one arrives at

$$\delta\omega'_c = \frac{\omega_2}{8} \left(\frac{m_*}{m\xi_2} \right)^2. \quad (5)$$

This expression exhibits a surprising trend of the width with respect to the particle energy. In contrast to CS, the harmonics become narrower for increasing electron energy, confirmed also with numerical calculations [55]. In the considered parameter regime $\omega_0/\delta\omega'_c \gg 1$, which results in an enhancement of satellite peaks over the spectral CS envelope. In fact, adding the second laser ξ_2 to the CS setup, new satellite peaks arise with a separation of ω_0 , and the smooth energy distribution within a large BW of CS, $\delta\omega'_{CS} \sim \omega_0\gamma^2/\xi_1^2$ [55], roams into sharp spikes.

The second contribution to the harmonic width arises from the finite duration effect of the laser pulse. One should note that the duration of the first pulse should be much longer, $N_1 = nN_2$, where $n = \omega_1/\omega_2$, and $N_{1,2}$ are the number of cycles in the pulses. This is to allow the electron to experience the full cycles of both pulses. Therefore, the photon uncertainty width is mostly determined by the second pulse, yielding the BW

$$\delta\omega'_f = 2\gamma_*^2\omega_2/N_2 = \omega_0/N_2. \quad (6)$$

Controlling the angle range θ_w , one can tune $\delta\omega'_w$ mentioned above not to exceed the dynamical width: $\delta\omega'_{in} =$

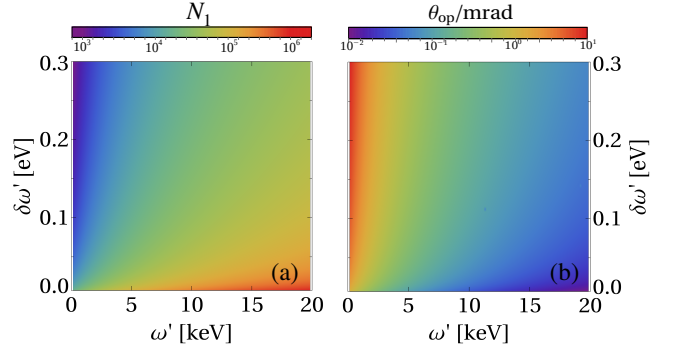


Figure 4. (a) the required pulse length N_1 of the ξ_1 laser for different emitted photon energies ω' with different harmonic peak widths $\delta\omega'$ in the spectrum. (b) the optimized angle range θ_{op} for different emitted photon energies ω' with different harmonic peak widths $\delta\omega'$ when we choose the pulse length in panel (b).

$\max(\delta\omega'_c, \delta\omega'_f)$.

The interplay between different BW contributions for different electron energies and emitted angle ranges is demonstrated in Fig. 3. In case I, $m_*/(m\xi_2) \gg 1$, and $\delta\omega'_{in} \approx \omega'_c \sim \omega_0$, i.e., the dynamical BW $\delta\omega'_{in}$ is of the same order of magnitude of the spacing $\Delta\omega' = \omega_0$ between two peaks, in the energy domain we are interested in. Hence, enlarging $\delta\omega'_w$ (through the particle energy) results in gradually widening the peak. A different behaviour is seen for case II [Lower panel in Fig. 3], when $\delta\omega'_{in} \approx \delta\omega'_f \ll \omega_0$, i.e., the dynamical BW $\delta\omega'_{in}$ is much smaller than the spacing. Since $\delta\omega'_f$ does not depend on the energy and angle, the line widths in the lower panel originate from $\delta\omega'_w \sim \gamma^2$. The latter increases with energy surpassing $\delta\omega'_{in}$ at $\varepsilon \gtrsim 30m$. As a result, a noisy background emission appears at the tail of the harmonic line, given by the Bessel function's rapid oscillations [55]. By scanning over both ε and θ , it can be shown that the larger the electron energy, the smaller the angle should be such that the isolated peaks are sharp enough for applications, see in [55]. We point out that for both cases in Fig. 3 the relative BW of the harmonics in the spectra can be as small as 10^{-4} for the comb (case II) and 10^{-5} for the single peak spectrum (case I), which is similar or even smaller compared with that of the XFEL beam [56].

Summarizing our approach, firstly, configuration I or II is chosen depending on the preference of the spectral shape: a single peak or a frequency comb. Then, the desired energy location and width should be specified. Employing Eq. (2), the energy ω' determines the effective relativistic factor γ_* . Then, from the chosen width $\delta\omega'$ and relation (3), the angle window θ_w follows. For case II, where $\delta\omega'_f$ dominates $\delta\omega'_{in}$, we also require $\delta\omega'_f = \delta\omega'$, from which the number of cycles in the second pulse is evaluated. For a given laser pulse energy the pulse length fixes the field amplitude. From the latter the effective mass is evaluated and from γ_* one finds the electron beam energy, see Fig. 4. For a given BW, the number of cycles is determined according to Eq. (6). However, increasing ω' requires a longer duration of the first pulse, due to increase of

$n = \omega_1/\omega_2 \approx 4\gamma_*^2$. The optimal angle window θ_w according to Eq. (2) is narrower at higher ω' .

In conclusion, the discussed CPW setup allows to generate an extremely narrow band and collimated x-ray beam in the range of several hundreds of eV to tens of keV, with brilliance by orders of magnitude exceeding that for CS corresponding to the same electron and laser parameters. By tuning the intensity of the two laser pulses, one can produce either a single peak or a comb-like x-ray source. Simple analytical expressions relating the source parameters (energy location, number of harmonic in comb, spectral width) to the laser and electron ones are provided. This radiation source is attractive for several applications. First, its narrow-band feature allows for resonant excitation spectroscopy of highly charged ions [40, 41], without the use of a monochromator as opposed to synchrotron sources. Second, the flux and BW of this source render it suitable to operate as an XFEL seeder, thus replacing the complex and cumbersome self-seeding unit [56–58], which is the only available seeding technique above energies of 100 eV. Third, owing to the low angle spread it is favourable as a source for small angle scattering diagnostics [38]. Fourth, the comb-like structure can be employed for extension of plasma spectroscopy from the optical and UV range to the hard x-ray domain, and for plasma diagnostics, e.g., for measuring the density profile of overdense plasmas. Finally, the achieved unprecedented parameters of the comb-like structure may pave the way to a hard x-ray frequency comb for ultrahigh precision metrology.

* qingzheng.lyu@mpi-hd.mpg.de

† erez.raicher@mail.huji.ac.il

- [1] B. M. Murphy O. H. Seeck, ed., *X-ray diffraction: Modern experimental technique* (Taylor and Francis Group, 2014) p. 420.
- [2] Carlos Sanchez-Cano, Ramon A. Alvarez-Puebla, John M. Abendroth, Tobias Beck, Robert Blick, Yuan Cao, Frank Caruso, Indranath Chakraborty, Henry N. Chapman, Chunying Chen, Bruce E. Cohen, Andre L. C. Conceição, David P. Cormode, Daxiang Cui, Kenneth A. Dawson, Gerald Falkenberg, Chunhai Fan, Neus Feliu, Mingyuan Gao, Elisabetta Gargioni, Claus-C. Glüer, Florian Grüner, Moustapha Hassan, Yong Hu, Yalan Huang, Samuel Huber, Nils Huse, Yanan Kang, Ali Khademhosseini, Thomas F. Keller, Christian Körnig, Nicholas A. Kotov, Dorota Koziej, Xing-Jie Liang, Beibei Liu, Sijin Liu, Yang Liu, Ziyao Liu, Luis M. Liz-Marzán, Xiaowei Ma, Andres Machicote, Wolfgang Maison, Adrian P. Mancuso, Saad Megahed, Bert Nickel, Ferdinand Otto, Cristina Palencia, Sakura Pascarelli, Arwen Pearson, Oula Peñate-Medina, Bing Qi, Joachim Rädler, Joseph J. Richardson, Axel Rosenhahn, Kai Rothkamm, Michael Rübhausen, Milan K. Sanyal, Raymond E. Schaak, Heinz-Peter Schlemmer, Marius Schmidt, Oliver Schmutzler, Theo Schotten, Florian Schulz, A. K. Sood, Kathryn M. Spiers, Theresa Staufer, Dominik M. Stemer, Andreas Stierle, Xing Sun, Gohar Tsakanova, Paul S. Weiss, Horst Weller, Fabian Westermeier, Ming Xu, Huijie Yan, Yuan Zeng, Ying Zhao, Yuliang Zhao, Dingcheng Zhu, Ying Zhu, and Wolfgang J. Parak, “X-ray-Based Techniques to Study the Nano–Bio Interface,” *ACS Nano* **15**, 3754–3807 (2021).
- [3] I. M. Ternov, “Synchrotron radiation,” *Sov. Phys.-Uspekhi* **38**, 409–434 (1995).
- [4] K Wille, “Synchrotron radiation sources,” *Reports on Progress in Physics* **54**, 1005–1067 (1991).
- [5] T Nakazato, M Oyamada, N Niimura, S Urasawa, O Konno, A Kagaya, R Kato, T Kamiyama, Y Torizuka, T Nanba, *et al.*, “Observation of coherent synchrotron radiation,” *Physical review letters* **63**, 1245 (1989).
- [6] H.-P. Schlenvoigt, K. Haupt, A. Debus, F. Budde, O. Jäckel, S. Pfotenhauer, H. Schwoerer, E. Rohwer, J. G. Gallacher, E. Brunetti, R. P. Shanks, S. M. Wiggins, and D. A. Jaroszynski, “A compact synchrotron radiation source driven by a laser-plasma wakefield accelerator,” *Nature Phys.* **4**, 130 (2008).
- [7] Henry N. Chapman, “X-ray imaging beyond the limits,” *Nature Materials* **8**, 299–301 (2009).
- [8] C Pellegrini, A Marinelli, and S Reiche, “The physics of x-ray free-electron lasers,” *Reviews of Modern Physics* **88**, 015006 (2016).
- [9] Christoph Bostedt, Sébastien Boutet, David M Fritz, Zhirong Huang, Hae Ja Lee, Henrik T Lemke, Aymeric Robert, William F Schlotter, Joshua J Turner, and Garth J Williams, “Linac coherent light source: The first five years,” *Reviews of Modern Physics* **88**, 015007 (2016).
- [10] The European X-Ray Laser Project XFEL, (2011).
- [11] The Linac Coherent Laser Source (LCLS), (2011).
- [12] Zhefang Zhao, Dong Wang, Qiang Gu, Lixin Yin, Guoping Fang, Ming Gu, Yongbin Leng, Qiaogen Zhou, Bo Liu, Chuanxiang Tang, *et al.*, “Sxfel: A soft x-ray free electron laser in china,” *Synchrotron Radiation News* **30**, 29–33 (2017).
- [13] A. Ting, R. Fischer, A. Fisher, K. Evans, R. Burris, J. Krall, E. Esarey, and P. Sprangle, “Observation of 20 ev x-ray generation in a proof-of-principle laser synchrotron source experiment,” *J. Appl. Phys.* **78** (1995).
- [14] R. W. Schoenlein, W. P. Leemans, A. H. Chin, P. Volfbeyn, T. E. Glover, P. Balling, M. Zolotarev, K.-J. Kim, S. Chattopadhyay, and C. V. Shank, “Femtosecond x-ray pulses at 0.4 Å generated by 90° thomson scattering: A tool for probing the structural dynamics of materials,” *Science* **274**, 236–238 (1996).
- [15] I. Sakai, T. Aoki, K. Dobashi, M. Fukuda, A. Higurashi, T. Hirose, T. Iimura, Y. Kurihara, T. Okugi, T. Omori, J. Urakawa, M. Washio, and K. Yokoya, “Production of high brightness gamma-rays through backscattering of laser photons on high-energy electrons,” *Phys. Rev. ST AB* **6**, 091001 (2003).
- [16] David J. Gibson, Scott G. Anderson, Christopher P. J. Barty, Shawn M. Betts, Rex Booth, Winthrop J. Brown, John K. Crane, Robert R. Cross, David N. Fittinghoff, Fred V. Hartemann, Jaroslav Kuba, Gregory P. Le Sage, Dennis R. Slaughter, Aaron M. Tremaine, Alan J. Wootton, Edward P. Hartouni, Paul T. Springer, and James B. Rosenzweig, “Pleiades: A picosecond Compton scattering x-ray source for advanced backlighting and time-resolved material studies,” *Phys. Plasmas* **11**, 2857–2864 (2004).
- [17] Antoine Rousse, Kim Ta Phuoc, Rahul Shah, Alexander Pukhov, Eric Lefebvre, Victor Malka, Sergey Kiselev, Frédéric Burgy, Jean-Philippe Rousseau, Donald Umstadter, and Danièle Hulin, “Production of a keV x-ray beam from synchrotron radiation in relativistic laser-plasma interaction,” *Phys. Rev. Lett.* **93**, 135005 (2004).
- [18] S. Corde, K. Ta Phuoc, G. Lambert, R. Fitour, V. Malka, A. Rousse, A. Beck, and E. Lefebvre, “Femtosecond x rays from laser-plasma accelerators,” *Rev. Mod. Phys.* **85**, 1–48 (2013).
- [19] Alberto Benedetti, Matteo Tamburini, and Christoph H Keitel, “Giant collimated gamma-ray flashes,” *Nature Photonics* **12**, 319–323 (2018).
- [20] Archana Sampath, Xavier Davoine, Sébastien Corde, Laurent

- Gremillet, Max Gilljohann, Maitreyi Sangal, Christoph H Keitel, Robert Ariniello, John Cary, Henrik Ekerfelt, *et al.*, “Extremely dense gamma-ray pulses in electron beam-multifoil collisions,” *Physical Review Letters* **126**, 064801 (2021).
- [21] Frederic V Hartemann, F  licie Albert, Craig W Siders, and C.P.J. Barty, “Low-intensity nonlinear spectral effects in compton scattering,” *Physical review letters* **105**, 130801 (2010).
- [22] Geoffrey A Krafft and Gerd Priebe, “Compton sources of electromagnetic radiation,” *Reviews Of Accelerator Science And Technology: Volume 3: Accelerators as Photon Sources*, 147–163 (2010).
- [23] Chao Chang, Chuanxiang Tang, and Juhao Wu, “High-gain thompson-scattering x-ray free-electron laser by time-synchronic laterally tilted optical wave,” *Phys. Rev. Lett.* **110**, 064802 (2013).
- [24] S. Chen, N. D. Powers, I. Ghebregziabher, C. M. Maharjan, C. Liu, G. Golovin, S. Banerjee, J. Zhang, N. Cunningham, A. Moorti, S. Clarke, S. Pozzi, and D. P. Umstadter, “Mev-energy x rays from inverse compton scattering with laser-wakefield accelerated electrons,” *Phys. Rev. Lett.* **110**, 155003 (2013).
- [25] Fred V. Hartemann and Sheldon S. Q. Wu, “Nonlinear brightness optimization in compton scattering,” *Phys. Rev. Lett.* **111**, 044801 (2013).
- [26] G. Sarri, D. J. Corvan, W. Schumaker, J. M. Cole, A. Di Piazza, H. Ahmed, C. Harvey, C. H. Keitel, K. Krushelnick, S. P. D. Mangles, Z. Najmudin, D. Symes, A. G. R. Thomas, M. Yeung, Z. Zhao, and M. Zepf, “Ultrahigh brilliance multi-mev gamma-ray beams from nonlinear relativistic thomson scattering,” *Phys. Rev. Lett.* **113**, 224801 (2014).
- [27] K. Khrennikov, J. Wenz, A. Buck, J. Xu, M. Heigoldt, L. Veisz, and S. Karsch, “Tunable all-optical quasimonochromatic thomson x-ray source in the nonlinear regime,” *Phys. Rev. Lett.* **114**, 195003 (2015).
- [28] Bal  sa Terzi  , Kirsten Deitrick, Alicia S Hofler, and Geoffrey A Krafft, “Narrow-band emission in thomson sources operating in the high-field regime,” *Physical review letters* **112**, 074801 (2014).
- [29] D Seipt, SG Rykovanov, A Surzhykov, and S Fritzsche, “Narrowband inverse compton scattering x-ray sources at high laser intensities,” *Physical Review A* **91**, 033402 (2015).
- [30] Vasily Yu Kharin, Daniel Seipt, and Sergey G Rykovanov, “Higher-dimensional caustics in nonlinear compton scattering,” *Physical review letters* **120**, 044802 (2018).
- [31] C Maroli, V Petrillo, I Drebot, L Serafini, B Terzi  , and GA Krafft, “Compensation of non-linear bandwidth broadening by laser chirping in thomson sources,” *Journal of Applied Physics* **124**, 063105 (2018).
- [32] Daniel Seipt, Vasily Yu Kharin, and Sergey G Rykovanov, “Optimizing laser pulses for narrow-band inverse compton sources in the high-intensity regime,” *Physical review letters* **122**, 204802 (2019).
- [33] MA Valialshchikov, V Yu Kharin, and SG Rykovanov, “Narrow bandwidth gamma comb from nonlinear compton scattering using the polarization gating technique,” *Physical Review Letters* **126**, 194801 (2021).
- [34] A.D. Debus, M. A Bussmann, M. A Siebold, A. A Jochmann, U. A Schramm, T.E. A Cowan, and R. A Sauerbrey, “Traveling-wave thomson scattering and optical undulators for high-yield euv and x-ray sources,” *Appl. Phys. B* **100**, 61 (2010).
- [35] A. Jochmann, A. Irman, M. Bussmann, J. P. Couperus, T. E. Cowan, A. D. Debus, M. Kuntzsch, K. W. D. Ledingham, U. Lehnert, R. Sauerbrey, H. P. Schlenvoigt, D. Seipt, Th. St  hler, D. B. Thorn, S. Trotsenko, A. Wagner, and U. Schramm, “High resolution energy-angle correlation measurement of hard x rays from laser-thomson backscattering,” *Phys. Rev. Lett.* **111**, 114803 (2013).
- [36] Frank E Carroll, Marcus H Mendenhall, Robert H Traeger, Charles Brau, and James W Waters, “Pulsed tunable monochromatic x-ray beams from a compact source: new opportunities,” *American journal of roentgenology* **181**, 1197–1202 (2003).
- [37] DCF Wieland, MA Schroer, A Yu Gruzinov, CE Blanchet, CM Jeffries, and DI Svergun, “Asaxs measurements on ferritin and apoferritin at the biosaxs beamline p12 (petra iii, desy),” *Journal of Applied Crystallography* **54** (2021).
- [38] Tao Li, Andrew J Senesi, and Byeongdu Lee, “Small angle x-ray scattering for nanoparticle research,” *Chemical reviews* **116**, 11128–11180 (2016).
- [39] Greg L Hura, Angeli L Menon, Michal Hammel, Robert P Rambo, Farris L Poole II, Susan E Tsutakawa, Francis E Jenney Jr, Scott Classen, Kenneth A Frankel, Robert C Hopkins, *et al.*, “Robust, high-throughput solution structural analyses by small angle x-ray scattering (saxs),” *Nature methods* **6**, 606–612 (2009).
- [40] Sven Bernitt, GV Brown, Jan K Rudolph, R Steinbr  gge, A Graf, M Leutenegger, SW Epp, Sita Eberle, K Kubi  ek, Volkhard M  ckel, *et al.*, “An unexpectedly low oscillator strength as the origin of the fe xvii emission problem,” *Nature* **492**, 225–228 (2012).
- [41] Steffen K  hn, Chintan Shah, Jos   R Crespo L  pez-Urrutia, Keisuke Fujii, Ren   Steinbr  gge, Jakob Stierhof, Moto Togawa, Zolt  n Harman, Natalia S Oreshkina, Charles Cheung, *et al.*, “High resolution photoexcitation measurements exacerbate the long-standing fe xvii oscillator strength problem,” *Physical review letters* **124**, 225001 (2020).
- [42] Thomas J B  rvenich, J  rg Evers, and Christoph H Keitel, “Nuclear quantum optics with x-ray laser pulses,” *Physical review letters* **96**, 142501 (2006).
- [43] Ralf R  hlsberger, Hans-Christian Wille, Kai Schlage, and Balaram Sahoo, “Electromagnetically induced transparency with resonant nuclei in a cavity,” *Nature* **482**, 199–203 (2012).
- [44] K P Heeg, A Kaldun, C Strohm, P Reiser, C Ott, R Subramanian, D Lentrodt, J Haber, H-C Wille, S Goerttler, R R  ffler, C H Keitel, R R  hlsberger, T Pfeifer, and J Evers, “Spectral narrowing of x-ray pulses for precision spectroscopy with nuclear resonances,” *Science (New York, N.Y.)* **357**, 375–378 (2017).
- [45] Kilian P. Heeg, Andreas Kaldun, Cornelius Strohm, Christian Ott, Rajagopalan Subramanian, Dominik Lentrodt, Johann Haber, Hans-Christian Wille, Stephan Goerttler, Rudolf R  ffler, Christoph H. Keitel, Ralf R  hlsberger, Thomas Pfeifer, and J  rg Evers, “Coherent X-ray-optical control of nuclear excitons,” *Nature* **590**, 401–404 (2021).
- [46] Farit Vagizov, Vladimir Antonov, YV Radeonychev, RN Shakhmurov, and Olga Kocharovskaya, “Coherent control of the waveforms of recoilless γ -ray photons,” *Nature* **508**, 80–83 (2014).
- [47] V. N. Baier, V. M. Katkov, and V. M. Strakhovenko, *Electromagnetic Processes at High Energies in Oriented Single Crystals* (World Scientific, Singapore, 1994).
- [48] Q. Z. Lv, E. Raicher, C. H. Keitel, and K. Z. Hatsagortsyan, “Anomalous violation of the local constant field approximation in colliding laser beams,” *Physical Review Research* **3**, 013214 (2021).
- [49] Q Z Lv, E Raicher, C H Keitel, and K Z Hatsagortsyan, “Ultra-relativistic electrons in counterpropagating laser beams,” *New Journal of Physics* **23**, 065005 (2021).
- [50] J. D. Jackson, *Classical Electrodynamics* (Wiley, New York, 1975).
- [51] Christoph Gohle, Thomas Udem, Maximilian Herrmann, Jens Rauschenberger, Ronald Holzwarth, Hans A. Schuessler, Ferenc

- Krausz, and T W Hänsch, “A frequency comb in the extreme ultraviolet,” *Nature* **436**, 234–237 (2005).
- [52] Arman Cingöz, Dylan C. Yost, Thomas K. Allison, Axel Ruehl, Martin E. Fermann, Ingmar Hartl, and Jun Ye, “Direct frequency comb spectroscopy in the extreme ultraviolet,” *Nature* **482**, 68–71 (2012).
- [53] Stefano M. Cavaletto, Zoltán Harman, Christian Ott, Christian Buth, Thomas Pfeifer, and Christoph H. Keitel, “Broadband high-resolution X-ray frequency combs,” *Nature Photonics* **8**, 520–523 (2014).
- [54] Gil Porat, Christoph M. Heyl, Stephen B. Schoun, Craig Benko, Nadine Dörre, Kristan L. Corwin, and Jun Ye, “Phase-matched extreme-ultraviolet frequency-comb generation,” *Nature Photonics* **12**, 387–391 (2018).
- [55] See the Supplemental Materials for the details.
- [56] Ichiro Inoue, Taito Osaka, Toru Hara, Takashi Tanaka, Takahiro Inagaki, Toru Fukui, Shunji Goto, Yuichi Inubushi, Hiroaki Kimura, Ryota Kinjo, *et al.*, “Generation of narrow-band x-ray free-electron laser via reflection self-seeding,” *Nature Photonics* **13**, 319–322 (2019).
- [57] Inhyuk Nam, Chang-Ki Min, Bonggi Oh, Gyujin Kim, Donghyun Na, Young Jin Suh, Haeryong Yang, Myung Hoon Cho, Changbum Kim, Min-Jae Kim, *et al.*, “High-brightness self-seeded x-ray free-electron laser covering the 3.5 keV to 14.6 keV range,” *Nature Photonics* , 1–7 (2021).
- [58] E Allaria, D Castronovo, P Cinquegrana, P Craievich, Massimo Dal Forno, MB Danailov, G D’Auria, A Demidovich, G De Ninno, S Di Mitri, *et al.*, “Two-stage seeded soft-x-ray free-electron laser,” *Nature Photonics* **7**, 913–918 (2013).

Supplemental Materials to the paper

"High-brilliance ultra-narrow-band x-rays via electron radiation in colliding laser pulses"

Q. Z. Lv,^{1,*} E. Raicher,^{2,†} C. H. Keitel,¹ and K. Z. Hatsagortsyan¹

¹Max-Planck-Institut für Kernphysik, Saupfercheckweg 1, 69117 Heidelberg, Germany

²Soreq Nuclear Research Center, 81800 Yavne, Israel

I. THE STRUCTURE OF THE HARMONICS

In this section, the details of the analytical estimations regarding the structure of harmonics, for example the harmonic width, the energy range of the x-ray comb and the optimized emitted angle, are presented. All the estimations are based on the analytical formula of the emission spectrum as well as the energy conservation law, which is well documented in our previous works [1, 2], and also verified by the numerical results in the main text.

The explicit formula for the radiation spectrum in general EM fields reads [3]:

$$dI = \frac{\alpha}{(2\pi)^2 \tau} \left[-\frac{\varepsilon'^2 + \varepsilon^2}{2\varepsilon'^2} |\mathcal{T}_\mu|^2 + \frac{m^2 \omega^2}{2\varepsilon'^2 \varepsilon^2} |\mathcal{I}|^2 \right] d^3 \mathbf{k}', \quad (1)$$

where $\mathcal{I} \equiv \int_{-\infty}^{\infty} e^{i\psi} dt$ and $\mathcal{T}_\mu \equiv \int_{-\infty}^{\infty} v_\mu(t) e^{i\psi} dt$ with $\psi \equiv \frac{\varepsilon}{\varepsilon'} \mathbf{k}' \cdot \mathbf{x}(t)$ being the emission phase and x_μ , v_μ , $k'_\mu = (\omega', \mathbf{k}')$ the four-vectors of the electron coordinate, the velocity and the photon momentum, respectively. τ is the pulse duration. For simplicity, the average energy is ε , and $\varepsilon' = \varepsilon - \omega'$.

Let us first look at the phase ψ of the emission, which is a crucial parameter in the formalism and determines the structure of the harmonics of the spectrum,

$$\begin{aligned} \psi &= \frac{\varepsilon}{\varepsilon'} \mathbf{k}' \cdot \mathbf{x}(t) \\ &= \psi_{np} t - z_2 \sin(\omega_2 t) - z_1 \sin(\omega_1 t) - z_{12} \sin(\Delta\omega_{12} t). \end{aligned} \quad (2)$$

Introducing the definition of $u = \omega'/\varepsilon'$, $\omega_1 = (1 + v_z)\omega_0$, $\omega_2 = (1 - v_z)\omega_0$ and $\Delta\omega_{12} = \omega_2 - \omega_1$ with v_z being the average velocity on axis, we may write

$$\begin{aligned} \psi_{np} &\equiv \varepsilon u (1 - v_z \cos \theta), \quad z_1 \equiv \frac{m u \xi_1}{\omega_1} \sin \theta, \\ z_2 &\equiv \frac{m u \xi_2}{\omega_2} \sin \theta, \quad z_3 \equiv \frac{2\omega_0 m^2 u \xi_1 \xi_2}{\varepsilon \Delta\omega_{12}^2} \cos \theta. \end{aligned} \quad (3)$$

With the analytical solution of the time integral in Eq. (1), one obtains

$$\mathcal{T}_\mu = 2\pi \sum_{s_1} \sum_{s_2} \mathcal{M}_\mu(s_1, s_2, \omega', \cos \theta) \delta(\Omega_{s_1, s_2}), \quad (4)$$

where s_1 and s_2 denote the absorbed photon number from ξ_1 and ξ_2 pulse, respectively. The matrix elements can be expressed

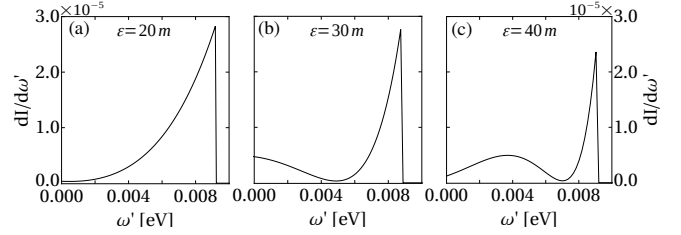


Figure S1. The spectra according to the analytical expressions of Eq. (1) for $\xi_1 = 0.1$ and $\xi_2 = 2$ with different energies. In order to show the narrow width of the peaks, the x-axis has been shifted to the right by 494.928 eV for (a), by 1103.835 eV for (b) and by 1982.290 eV for (c). Here the spectra are calculated by the analytical formulas in Ref. [2].

as the multiplication of Bessel functions with arguments z_1 , z_2 , z_3 [2]. Furthermore, based on the argument of the δ -function, the energy conservation can be written as

$$\begin{aligned} \omega' &= \frac{\varepsilon(s_1 \omega_1 + s_2 \omega_2)}{\varepsilon(1 - v_z \cos \theta) + (s_1 \omega_1 + s_2 \omega_2)} \\ &\approx \frac{2\gamma_*^2 (s_1 \omega_1 + s_2 \omega_2)}{1 + 2\gamma_*^2 (1 - \cos \theta)}, \end{aligned} \quad (5)$$

The last step is the approximation connected with neglect of the recoil. The emission is nearly on axis ($\theta \sim 0$) and can thus be confined to a small range $0 < \theta < \theta_w$. The width of the harmonic due to this finite angle window is $\delta\omega'_w = \omega'(\theta = 0) - \omega'(\theta = \theta_w)$. Employing Eq. (5) and Taylor expanding for $\theta \ll 1$ one obtains

$$\delta\omega'_w = \omega_{s_1, s_2}^m (\gamma_* \theta_w)^2. \quad (6)$$

where $\omega_{s_1, s_2}^m = 2\gamma_*^2 (s_1 \omega_1 + s_2 \omega_2)$ and $\gamma_* = \varepsilon/m_*$ with the effective mass $m_* \equiv m \sqrt{1 + \xi_1^2 + \xi_2^2}$.

As seen from the main text, the harmonics we are interested in is determined by the ξ_2 -laser co-propagating with the electrons. The structure of the harmonics are therefore related with z_2 and the corresponding Bessel functions as well as the emission angle θ . According to Eq. (5), the corresponding sine function is approximately given by $\sin \theta \approx \sqrt{1 - 1/v_z^2 + 2(s_1 \omega_1 + s_2 \omega_2)/(\varepsilon u v_z^2)}$. Substituting this expression into Eq. (3) one obtains

$$z_2 = \frac{\xi_2 m_* m}{\omega_2 \varepsilon} \sqrt{u(u_s - u)}, \quad (7)$$

where $u_s \equiv 2\varepsilon(s_1 \omega_1 + s_2 \omega_2)/m_*^2$. The main harmonics in Fig. 3 of the paper correspond to $s_1 = 1$ and $s_2 \sim 1$, which

* qingzheng.lyu@mpi-hd.mpg.de

† erez.raicher@mail.huji.ac.il

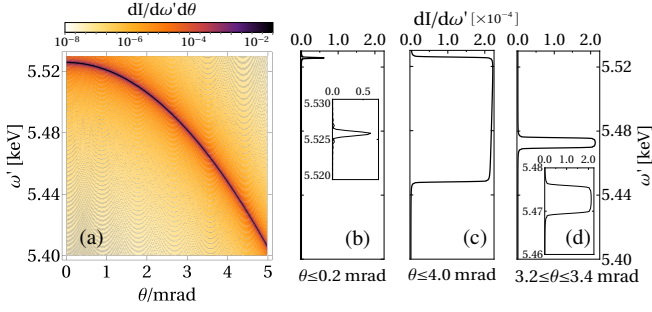


Figure S2. (a) the angle resolved spectrum for the common Compton scattering source with $\xi_1 = 0.1$; (b), (c) and (d) are the spectra for the same parameters but integrated over different angle spreading, (b) for $\theta \leq 0.2$ mrad, (c) for $\theta \leq 4.0$ mrad, and (d) for $3.2 \leq \theta \leq 3.4$ mrad. Please note that the radiation is around $\theta = \xi_1/\gamma \approx 3.3$ mrad. The other parameters are the same as in Fig. 2 in the paper.

means $u_s \approx 2\varepsilon\omega_1/m_*^2$. Then, the width δu can be estimated according to $z_2 \approx s_2$ in this regime and expressed as

$$\delta u = \frac{\omega_2^2 \varepsilon}{2\xi_2^2 \omega_1 m} . \quad (8)$$

Therefore, according to $u = \omega'/\varepsilon'$, the intrinsic width of the peak $\delta\omega'_c$ is approximately

$$\delta\omega'_c = \frac{\varepsilon^2 \omega_2^2}{2\xi_2^2 \omega_1 m^2 + \varepsilon \omega_2^2} \approx \frac{\omega_2}{8} \left(\frac{m_*}{m\xi_2} \right)^2 . \quad (9)$$

In the last step, we have neglected the photon recoil for simplicity. From this estimation, we can see that the width is decreasing with the increasing of the electron energy, seen in Fig. S1. According to Eq. (9), the full width at half maximum of the peak is 0.00313eV for panel (a), 0.00138eV for panel (b) and 0.00076eV for panel (c), which is approximately proportional to $1/\gamma_*^2$. This is in contrast with the width of the harmonic in the single plane wave case, where $\delta\omega' \sim \omega_0\gamma^2/\xi^2$ increases with the electron energy.

Meanwhile, we can also estimate the optimized emitted angle of the photons. Since the emission in our setup is almost on axis, the Bessel function arguments in Eq. (3) can thus be rewritten as $z_2 \approx m\xi_2 u\theta/\omega_2$. As the main peak appears when $u = u_s \approx 2\varepsilon\omega_1/m_*^2$ and $z_2 \sim 1$, the optimized angle θ_{op} is

$$\theta_{op} = \frac{m_*^2}{8\gamma\xi_2^2\varepsilon^2} , \quad (10)$$

which also decreases with the electron energy. This coincides with Fig. 4(b) in the main text. It is also worth to point out that this optimized angle is different from the scattering of an electron from circularly polarized plane wave laser pulse with the optimized emitted angle around ξ_1/γ .

From $z_2 \approx m\xi_2 u\theta/\omega_2$, we can also see that z_2 tends to 1 for the angle $\theta \sim 0$ as ω_2 being rather small. This explains the almost on axis emission in the CPW setup. In the opposite, the harmonics in the common CS, which triggered by ξ_1 only,

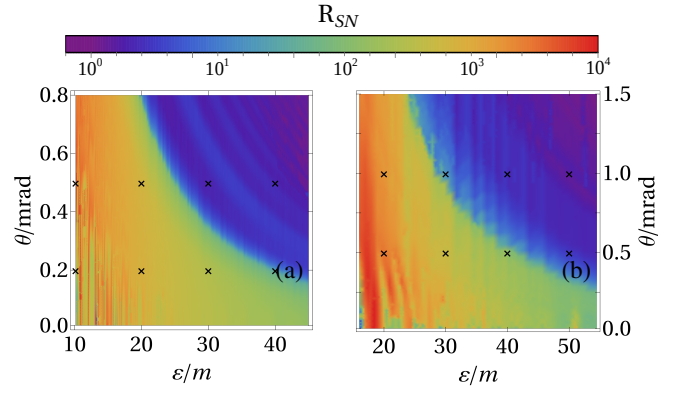


Figure S3. The signal-to-noise ratio R_{SN} vs ε and θ : (a) for $\xi_1 = 0.1$ and $\xi_2 = 0.02$ and (b) for $\xi_1 = 0.1$ and $\xi_2 = 2$. The pulse length for ξ_1 is $N_1 = 80000$ for both cases. The oscillations in the plot stem from the background emission which induces oscillations in I_{min} , especially for case II. The crosses show the parameters considered in Fig. 3 in the main text.

is determined by z_1 and thus the harmonics center for larger angles according to Eq. (3).

Another interesting property of the spectrum is the energy range of the x-ray comb for the case of $\xi_2 > \xi_1$. As explained in the paper, the peaks are equally distant with the laser basic frequency ω_0 , the estimation of this range is equivalent to estimating the number of peaks in the comb-like structure. The peaks are determined by Bessel functions with the argument of z_2 , the same as for the intrinsic width. It is well known that a Bessel function tends to be zero when the argument is much larger or smaller than the order of the function. Therefore, the peak appears only when $z_2/\Delta s_2 = \delta \sim 1$. With a given emitted angle window $0 < \theta < \theta_w$ as before, z_2 can be approximated as $2\xi_2\theta_w\varepsilon(\Delta s_2\omega_2 + \omega_1)/(\omega_2 m_*^2)$. Therefore, we can solve for Δs_2 based on $z_2 = \delta\Delta s_2$ and obtain

$$\Delta s_2 = \frac{2\xi_2\varepsilon\omega_1\theta_w}{\delta\omega_2 m_*^2 + 2\xi_2\varepsilon\omega_2\theta_w} \approx \frac{1}{\delta} \left(\frac{\theta_w}{\theta_c} \right) . \quad (11)$$

with $\theta_c = m_*/(8m\xi_2\gamma_*^3)$ according to $\delta\omega'_w(\theta_c) = \delta\omega'_c$. From this formula we can see that the number of peaks is proportional to the angle spreading θ_w of the radiation. If we choose the optimized angle in Eq. (10), Δs_2 is proportional to $1/\xi_2$, which means that by lowering the strength of ξ_2 -laser in the configuration, the range of the comb-like structure can be extended.

II. ANGULAR SPECTRUM FOR THE COMMON COMPTON SCATTERING SOURCE

In the main text, we have shown that the common Compton scattering (CS) source has a much wider spectrum compared to the CPW setup. In order to understand the underlying mechanism, the angular spectrum for a CS is displayed in Fig. S2. Panel (a) shows that the emitted photon energy coincides with Eq. (5) for $s_2 = 0$, which means the ξ_2 -laser is absent and the single harmonic is only according to $\xi_1 < 1$.

Panel (b) and (c) show the integrated spectrum for two different angle ranges for θ . In panel (b), we confine the angle in the same range as in Fig. 2(b) in the paper and the emitted spectrum obtained here is not only less intense but also much wider compared with Fig. 2(b) in the main text. If we want to have a similar BW as in Fig. 2(b) in the paper, the angle window for θ has to be decreased even more, which will make the intensity negligible. This is because the main radiation for the common CS is around ξ_1/γ and by integrating over a certain angle region which does not include $\xi_1/\gamma = 3.3$ mrad will give us weak radiation. Thus, the angle window in panel (c) is enlarged to 4 mrad and the intensity of the spectrum is now the same as in Fig. 2(b) in the paper but the relative width is several orders of magnitude larger than the one in the CPW setup. This is because the larger the angle, the stronger the emitted energy ω' depends on the angle as in Fig. S2, and thus the wider is the harmonic for the same angle range. This also explains that even when we integrate the same angle window as in the CPW case but around ξ_1/γ , the spectrum is still wider than the CPW spectrum, seen in Panel (d). The brilliance for this emission

is also smaller than the case in the CPW setup, because the emitted photons for a CS in Panel (d) not only distributes in a wider energy range but also is collected in a larger solid angle as $\theta \sim \xi_1/\gamma$, seen also Fig. 1(f) in the paper.

III. SIGNAL TO NOISY RATIO FOR THE CPW SETUP

In order to have a comprehensive picture of the impact of the electron energy and the emitted angle on the structure of the harmonics, we present, in this section, the signal to noise ratio, $R_{SN} = I_{max}/I_{min}$, for the two cases in Fig. S3(a) and (b). Here I_{max} is the intensity at the main peak, while I_{min} is the intensity at the middle point between the main peak and the adjacent one. By scanning over both ε and θ , we can see that the larger the electron energy, the smaller the angle should be such that the isolated peaks are sharp enough ($R_{SN} > 100$). The sudden jump in R_{SN} for both cases corresponds to the situation where the angle width reaches the middle point, $\delta\omega'_w = \omega_0/2$.

[1] Q. Z. Lv, E. Raicher, C. H. Keitel, and K. Z. Hatsagortsyan, “Anomalous violation of the local constant field approximation in colliding laser beams,” *Physical Review Research* **3**, 013214 (2021).

[2] Q Z Lv, E Raicher, C H Keitel, and K Z Hatsagortsyan, “Ultra-relativistic electrons in counterpropagating laser beams,” *New Journal of Physics* **23**, 065005 (2021).

[3] V. N. Baier, V. M. Katkov, and V. M. Strakhovenko, *Electromagnetic Processes at High Energies in Oriented Single Crystals* (World Scientific, Singapore, 1994).